Kinetics-assisted discrimination of active sites in Ru catalyzed hydrolytic dehydrogenation of ammonia borane

Wenzhao Fu[a,#], Wenyao Chen[a,#], Gang Qian[a], De Chen[b], Weikang Yuan[a], Xuezhi Duan[a,*], Xinggui Zhou[a]

[a] State Key Laboratory of Chemical Engineering, East China University of Science and Technology, 130 Meilong Road, Shanghai 200237, China

[b] Department of Chemical Engineering, Norwegian University of Science and Technology, Trondheim 7491, Norway

[#]These authors contributed equally to this work.

*Corresponding Author: xzduan@ecust.edu.cn; Tel.: +86-21-64250937; Fax.: +86-21-64253528

Abstract:

Identifying the underlying nature of the structure sensitivity from the catalyst active site point of view in heterogeneous catalytic reactions is of prime scientific and industrial importance. In this work, the kinetics-assisted discrimination of the active sites is explored in size-sensitive Ru catalyzed hydrolytic dehydrogenation of ammonia borane by combining multi-faceted kinetics analysis with model calculations. These differently sized Ru/CNTs catalysts employed are found to exist in the form of hcp crystal structure and truncated hexagonal bipyramid shape. The size-insensitive activation energies indicate that one typed Ru active sites mainly dominate the reaction, which are discriminated as the Ru edge atoms. Further combining kinetic isotopic analysis with DFT calculations suggests the favorable occurrence of the rate-determining step on such active sites. The insights revealed here could shed new light not only on how to achieve the kinetics-assisted discrimination of active sites for structure-sensitive reactions, but also on guiding the rational design and optimization of Ru catalysts for the reaction.

1 Introduction

It is well-known that catalysis is a kinetic phenomenon, and the reaction rate of a solid catalyst is equal to the sum of that of each active sites (e.g., terraced surfaces, stepped surfaces, edge atoms and corner atoms) in heterogeneous catalysis [1-5]. For most structure-sensitive reactions, an ideal strategy is to understand the underlying nature of the size-dependent catalytic activity toward rational design and optimization of catalysts [6-10], which is increasingly facilitated by multiple techniques, such as well-defined catalyst preparation, kinetic (isotopic) studies, surface science studies and theoretical calculations.

The probe reaction in this work is metal-catalyzed hydrolytic dehydrogenation of ammonia borane featuring a high hydrogen capacity of 19.6%, which is a well-known structure-sensitive reaction [2,11]. This has been increasingly attracted to produce hydrogen under mild reaction conditions for fuel cell applications [12,13]. Our recent kinetic and isotopic studies have evidenced that this reaction proceeds in terms of $NH_3BH_3+4H_2O\rightarrow NH_4^++B(OH)_4^-+3H_2\uparrow$ [14,15]. For this reaction, a large amount of metal components and supports have been tested [11,16,17], and carbonaceous nanomaterials supported noble metal catalysts have exhibited higher hydrogen generation activities [18-21]. Recently, mechanistic, structural and theoretical understanding of these catalytic systems are of growing interest with the aim to guide the rational design and optimization of catalysts [22-25]. Among them, our proposed method based on the multi-faceted kinetics analysis is simple yet effective to discriminate the dominant active sites of fcc Pt catalysts for the reaction [2]. As a

consecutive effort, we focus our attention on probing whether this method is applicable to discriminate the dominant active sites of hcp Ru catalysts for the reaction, and on further combining kinetic isotopic analysis with DFT calculations to obtain the mechanistic understanding of the discriminated active sites.

The objective of this study is to achieve the kinetics-assisted discrimination of the active sites for Ru catalyzed hydrolytic dehydrogenation of ammonia borane. The crystal phase, size and shape of Ru/CNTs catalysts were first characterized by X-ray diffraction (XRD), high angle annular dark field-scanning transmission electron microscopy (HAADF-STEM), high resolution transmission electron microscopy (HRTEM) and selected area electron diffraction (SAED). Subsequently, these differently sized catalysts were tested for the reaction, and then plotting the intrinsic catalytic activity, i.e., $TOF_{active\ site}$ based on the number of the active sites, with the Ru particle size was carried out by combining multi-faceted kinetics analysis with model calculations for discriminating the dominant active sites. Furthermore, the nature of the active sites was understood by combining kinetic isotopic analysis with DFT calculations. These results showed that the Ru edge atoms of hcp Ru/CNTs catalysts are dominant active sites for the reaction, and this has not been reported previously in the literature.

2 Experimental

2.1 Catalyst preparation

Pristine multi-walled carbon nanotubes (CNTs, purity>99.5%, purchased from Beijing

Cnano Technology Limited) with close ends were directly used to immobilize Ru catalysts with different loading, i.e., 0.5, 0.75, 1.5, 4.5 and 6.0 wt%, respectively. Typically, an aqueous solution of $RuCl_3$ (Sinopharm Chemical Reagent Co. Ltd) was mixed with CNTs by incipient wetness impregnation. The as-prepared precursors were dried under stagnant air at room temperature for 12 h followed by drying at 110 ºC for 12 h, and then reduced by a continuous H_2 flow at 250 ºC for 2 h (at 5 ºC·min^{-1}). After being cooled to room temperature under Ar atmosphere, the reduced catalysts were exposed to 1% O_2/Ar atmosphere for 20 min to form a passivation layer for prohibiting the bulk oxidation. The passivated catalysts were kept under an inert atmosphere before testing and characterizations, and denoted as Ru-x/CNT, in which x represents the weight percentage of metal.

2.2 Catalytic testing

Catalytic testing of the five catalysts for hydrolysis of ammonia borane was performed in a three-necked flask immersed in a water bath to control the temperature of the reaction solution with deviation of ±0.5ºC and placed on a magnetic stirrer at the stirring speed of 900rm, where any influence of external diffusion has been ruled out in our previous work [2]. For all the experiments, the weight ratio of ruthenium to ammonia borane was kept as 0.03:1. When the injection of AB solution (5 mL and 0.01 g·mL^{-1}) into the flask, the reaction started and a water-filled gas burette followed by an electronic balance was connected to the reaction flask. The volume of the evolved hydrogen gas was calculated by the weight of the discharged water by so-called water

displacement method.

The replacement of H_2O with D_2O as the reactant at the same reaction conditions was used to compare the difference ability of water activation over the five catalysts. Similarly, the same amount of catalysts was preloaded into the flask before the reaction and then a D_2O dissolved ammonia borane solution (5 mL and 0.01 $g \cdot mL^{-1}$) was injected into the flask via a syringe.

2.3 Catalyst characterization

HAADF-STEM investigation was carried out using a Tecnai G2 F20 S-Twin equipped with digitally processed STEM imaging system. The Ru particle sizes distributions over the five catalysts were determined by counting at least 200 random particles. XRD patterns were collected by Rigaku D/Max 2550VB/PC diffractometer using Cu K_α radiation. HRTEM images were obtained by a JEOL JSM-2100 electron microscope after mounting the sample on a carbon-coated copper grid (200 mesh) using ethanol dispersion.

3 Results and Discussion

3.1 The method to understand unique size-insensitive activation energy of Ru/CNT catalysts

Ru catalyzed hydrolytic dehydrogenation of ammonia borane has been known to be a typical structure sensitive reaction [11,26]. It is highly desirable to fundamentally understand the underlying nature of the Ru particle size dependent hydrogen generation

rate by combining multi-faceted kinetics analysis with model calculations, aiming to achieve the discrimination of dominant Ru active sites and then guide the rational catalyst design. As schematically shown in Fig. 1a and 1b, the multi-faceted kinetics analysis and the model calculations can give an expression about the E_a of Ru catalyst particles as a function of the y_i being the fraction of each typed active site and that about the y_i as a function of the Ru particle size ($d_{particle}$), respectively, where more details of equations derivation can refer to our previous work [2]. Notably, the y_i is difficult to be determined by experiments, while the E_a and Ru particle size can be easily determined. Therefore, by correlating the E_a with the $d_{particle}$, it is possible to understand the information of Ru active sites and then discriminate the dominant one/ones.

HAADF-STEM with high resolution was first employed to characterize the five catalysts, which can obtain reliable particle size distributions [27], and the results are shown in Fig. S1a-1f. Based on at least 200 random particles, their mean particle sizes are determined to be 1.0 ± 0.2, 1.2 ± 0.2, 1.4 ± 0.3, 1.6±0.3 and 1.8 ± 0.3 nm, respectively. Then, these Ru/CNTs catalysts were tested with the same molar ratio of AB to Ru under different reaction temperature. It is obviously seen in Fig. S2 that all the reactions follow linear relationships between the hydrogen generation volume and the reaction time in the initial period, e.g., the AB conversion being less than 50%, being indicative of the zero-order reaction characteristic [2]. Based on the slopes of hydrogen generation curves, the corresponding reaction rate constant (k) can be obtained. As shown in Fig. 1c, the logarithm of the as-obtained k was correlated with the reciprocal absolute temperature (1/T) to yield the corresponding E_a. Unexpectedly,

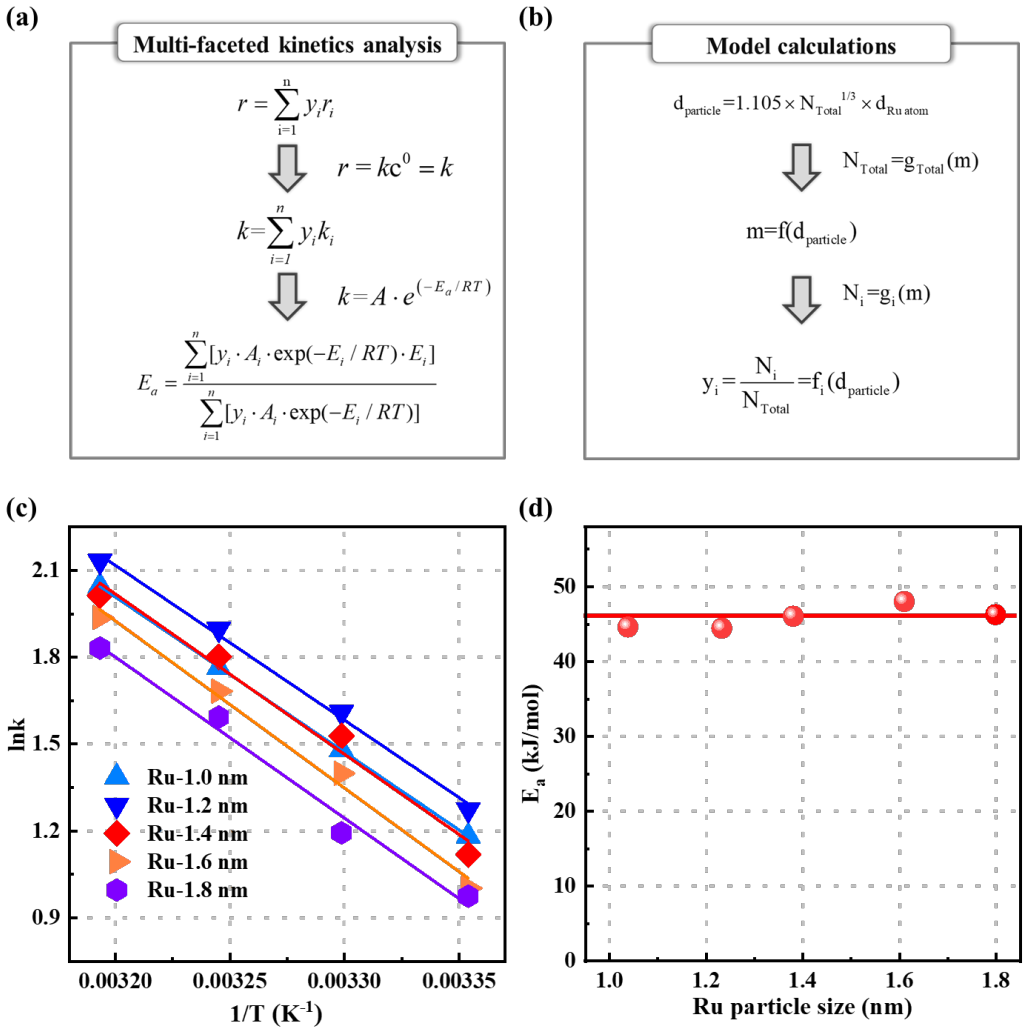

Fig. 1 (a) Scheme of the multi-faced kinetics analysis, where i is the type of the active site, y_i is the fraction of each typed active site per mole of Ru. (b) Scheme of the model calculations, where m means the number of atoms lying on an equivalent edge; N_i is the number of atoms for each typed active sites (e.g., corner, edge, 101 and 001) in each particle and it is a function of m. (c) ln *k*, derived from hydrogen generation rate versus reaction time, as a function of 1/T over differently sized Ru/CNT catalysts. (d) Activation energy as a function of Ru particle size.

as the Ru particle size increases, all the E_a values in Fig. 1d are found to be very similar,

which are in the range of 44-48 kJ/mol. This size-insensitive E_a strongly indicates that one typed active site, i.e., the y_i equaling to one, dominates the reaction, in which the E_a equals to E_1. Further assuming no obvious change in the activity of this typed active site with the Ru particle size, the corresponding turnover frequency ($TOF_{active\ site}$) would be size-insensitive, that is, the constant $TOF_{active\ site}$ regardless of the Ru particle size. Along this line, by correlating the $TOF_{active\ site}$ with the Ru particle size, it is easy to discriminate this typed active site for the reaction, i.e., the size-insensitive trend of $TOF_{active\ site}$ indicating that this specific active site should be the dominant one.

3.2 Discrimination of dominant Ru active sites

To address the above issue, the model calculations proposed above were first performed to obtain the number of each specific active site, which are based on the known Ru crystal phase and morphology. They were characterized by XRD and HRTEM, respectively. It can be seen in Fig. 2a that in addition to the characteristic diffraction peaks of CNTs (i.e., C (002) and C (101) at 26.6° and 44.0°, respectively), the CNT supported Ru nanoparticles show one legible diffraction peak at 38.4° assigned to the (100) of hcp Ru (JCPDS no. 06-0663). On a typical HRTEM image in Fig. 2b, the lattice fringe distances of 0.205 (± 0.003), 0.213 (± 0.003) and 0.233 (± 0.003) nm are found to be consistent with the theoretical values of 0.205, 0.214 and 0.234 nm for hcp Ru {101}, Ru {002} and Ru {100}, respectively [28,29]. Meanwhile, the CNT supported Ru nanoparticles almost exhibit a well-defined shape (Fig. S3). It can be observed in Fig. 2c that the fast Fourier transform (FFT) of the selected particle indicates the

electron diffraction pattern with an HCP crystal along the [010] zone axis. Moreover, the angles between the hcp Ru(101) and Ru(101), Ru(101) and Ru(002), and Ru(101) and Ru(100) are 58°, 62° and 29°, respectively [28-30]. This suggests the Ru nanoparticles exist in the form of a truncated hexagonal bipyramid shape, which is schematically

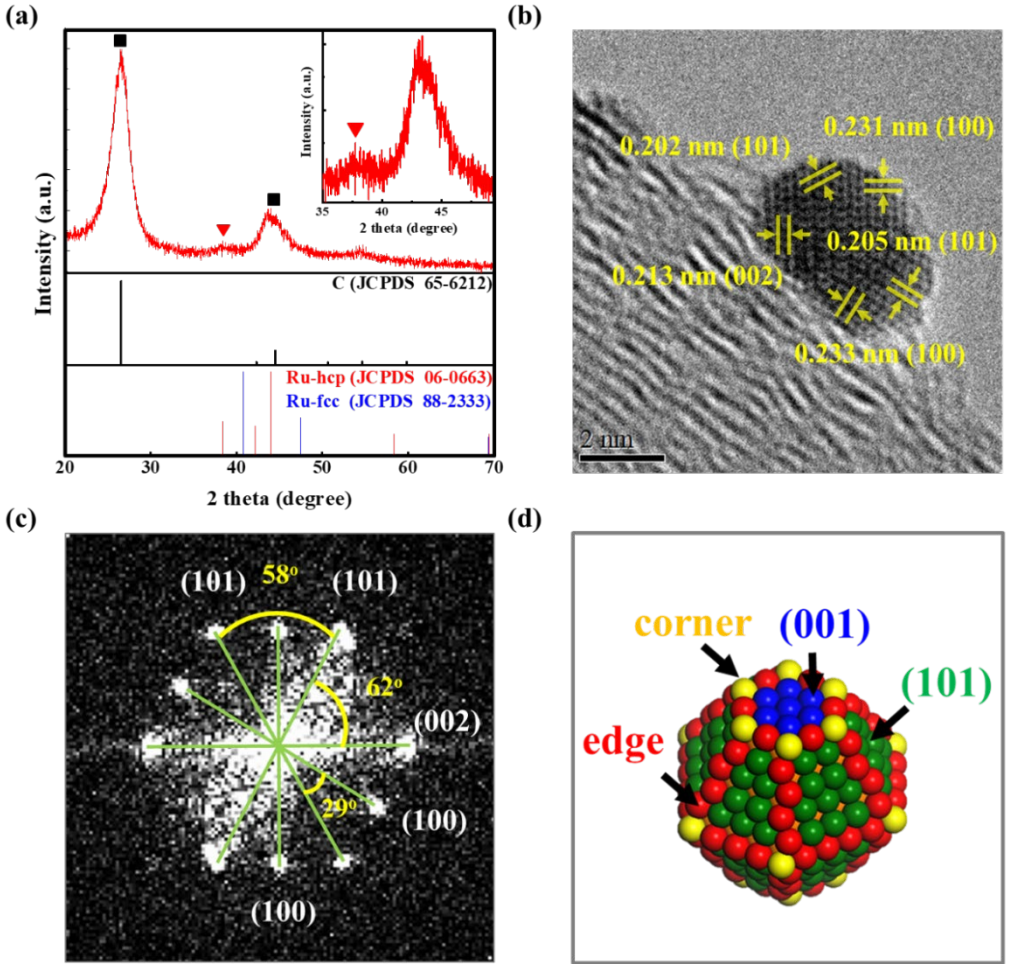

Fig. 2 (a) XRD pattern of typical Ru/CNT catalyst. The inset shows the enlarged pattern around 35-40°. Standard patterns of the carbon (▼, JCPDS no. 65-6212), the hcp Ru (●, JCPDS no. 06-0663) and the fcc Ru (JCPDS no. 88-2333) are presented to identify the crystal phases. (b and c) Typical HRTEM image of Ru/CNT catalyst, and its corresponding FFT pattern. (d) Schematic diagram of truncated hexagonal bipyramid.

shown in Fig. 2d with two {001} and twelve {101} facets [31]. Notably, when the Ru particle is supported on CNT, it would lie along the cone axis direction, where the four {101} facets are embedded in the CNT support.

With these identified Ru particle shape and sizes, the fractions of the corner, edge, (101) and (001) number to surface atoms in one specific sized Ru particle were obtained by formulas in Table S1. As shown in Fig. 3a, the fractions of surface, corner, (001) and (101) atoms show monotonical trends with the Ru particle size, while that of edge atoms with a volcano shape. Considering that the used mole of Ru in each reaction was kept with the same, different sized Ru catalysts correspond to different number of Ru nanoparticles for the given molar Ru. Therefore, the atom numbers of each specific active site per mole of Ru were calculated, and the results are presented in Fig. 3b. Taking the initial rates at 30°C as an example (Fig. 3c), the $TOF_{active\ site}$ can be obtained based on the data of Fig. 3b and 3c. For clear comparison, these data were normalized by normalizing each TOF point to its highest TOF for each typed active site, and the results are shown in Fig. 3d. Obviously, only when the Ru edge atoms are considered as the active sites, the correspondingly normalized $TOF_{active\ site}$ has a weak dependence on the Ru particle size, i.e., size-insensitive and constant $TOF_{active\ site}$ based on the Ru edge atoms. This strongly suggests that the edge atoms of Ru/CNT catalysts are dominant active sites for the reaction.

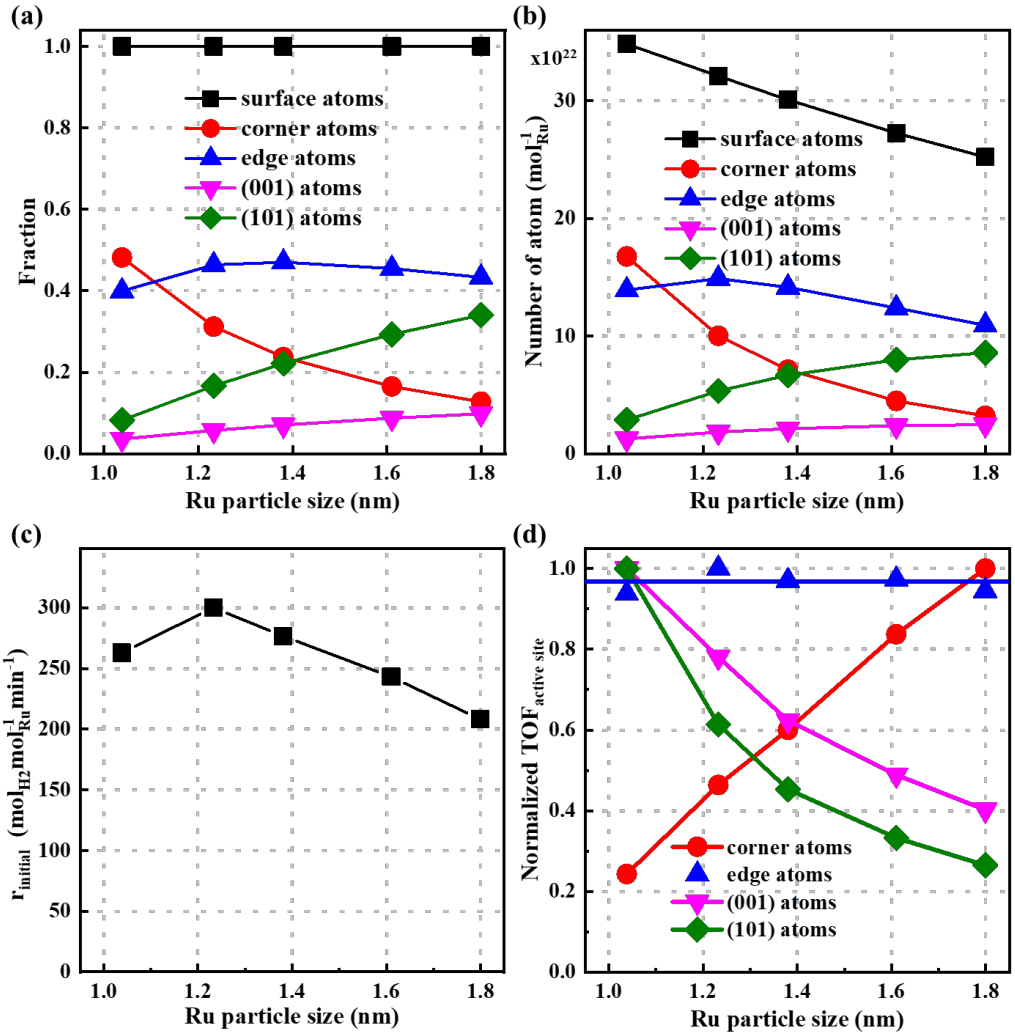

Fig. 3 (a) Plots of the fraction of each typed active site to the total surface atoms in one sized Ru particle with the Ru particle size. (b) Plots of the number of total surface atoms and each specific active site per mole of Ru with the Ru particle size. (c) The initial hydrogen generation rate ($r_{initial}$) at 30 °C as a function of the Ru particle size. (d) The calculated normalized $TOF_{active\ site}$ based on the number of corner, edge, (001) and (101) atoms with the Ru particle size.

It is noted that the above results show almost unchanged $TOF_{active\ site}$ of edge atoms over the differently sized Ru catalysts in Fig. 3d. This indicates that there is no obvious

change in the activity of the Ru active sites with the Ru particle size, i.e., these catalysts with similar Ru electronic properties, which can confirm the above assumption of the size-insensitive $TOF_{active\ site}$ for our proposed method by combining multi-faceted kinetics analysis with model calculations. Meanwhile, this also indicates that the origin of the size-dependent reaction rate in Fig. 3c and TOF_{app} in Fig. S4 based on the number of the total surface atoms mainly arises from the difference in the number of the Ru active sites, i.e., the Ru geometric properties, rather than that in the quality of the Ru active sites, i.e., the Ru electronic properties.

3.3 Kinetic isotopic and theoretical understanding for the nature of Ru active sites

As has been demonstrated above, the method by combining multi-faceted kinetics analysis with model calculations is very effective to discriminate the Ru edge atoms as the dominant active sites for the reaction. In order to reveal the nature of the Ru active sites, we resort to kinetic isotopic analysis and DFT calculations toward mechanistic and atomic-level understanding. Previous studies showed that no or small kinetic isotopic effects (KIE) of ammonia borane is observed, while remarkable KIE of water occurs [22]. KIE measurements of water for the five Ru/CNT catalysts in Fig. 4a show that all the catalysts exhibit much lower hydrogen generation rates when D_2O is used as the reactant. Their KIE values were determined by the ratio of the rate constants, i.e., k_H/k_D. As shown in Fig. 4b, they are 2.7, 2.6, 2.7, 2.7, and 2.8, respectively, which are classified as the primary kinetic isotopic effects [22,32]. This suggests the O-H bond cleavage in water molecule being in the rate determining step (RDS). Meanwhile,

similar KIE values of the five differently sized Ru/CNT catalysts also offer strong support for our above findings, i.e., these catalysts with almost the same Ru active sites and electronic properties.

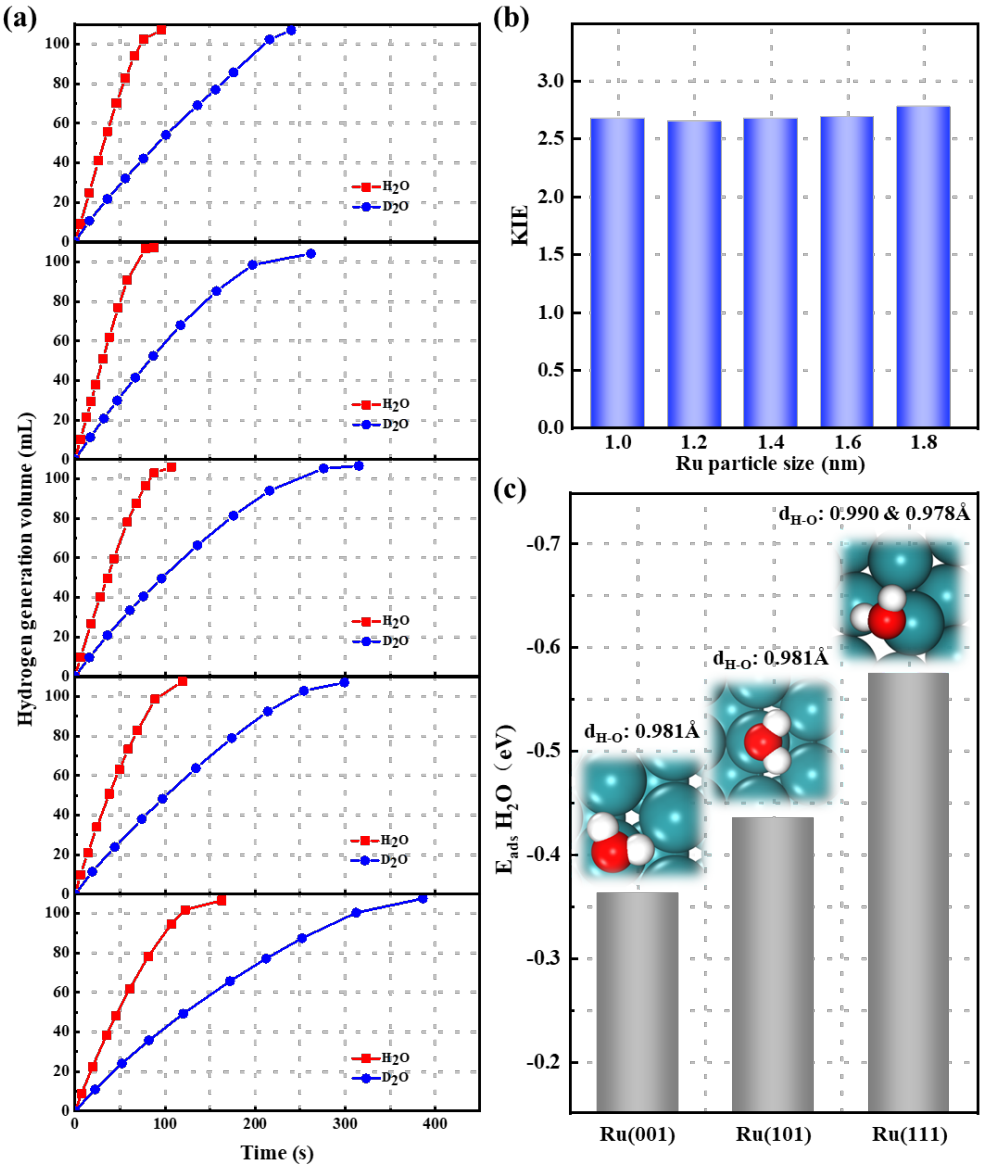

Fig. 4 (a) Hydrogen generation volume as a function of time using H_2O and D_2O as the reactants, from up-to-down are Ru-0.5, Ru-0.75, Ru-1.5, Ru-4.5, and Ru-6.0 catalysts, respectively. (b) Kinetic isotope effect (KIE) values of Ru-0.5, Ru-0.75, Ru-1.5, Ru-3.0, Ru-4.5, and Ru-6.0 catalysts. (c) The calculated H_2O adsorption energy and the H-O bond length for Ru(001), Ru(101) and Ru(111), respectively.

As a consecutive effort, DFT calculations were performed to understand the difference in the water adsorption behavior on three representative Ru surfaces, i.e., Ru (001), Ru (101) and Ru (111). It can be clearly seen in Fig. 4c that the stepped Ru (111) surface exhibit has higher water adsorption energy than the other two terraced surfaces. Meanwhile, the Ru(111) surface is observed to exhibit larger O-H bond elongation from 0.973Å for the free water to 0.990Å. This suggests stronger weakening of the O-H bond in the adsorbed water, which could provide an interpretation for the Ru edge atoms being the dominant active sites for the reaction.

Based on the above analyses, our proposed method, i.e., kinetics-assisted discrimination of catalyst active sites, is effective to discriminate the dominant active sites for the Ru-catalyzed hydrolytic dehydrogenation of ammonia borane. This method is based on plotting the $TOF_{active\ site}$ with the metal particle size to identify the size-insensitive $TOF_{active\ site}$ line and then discriminate this specific crystal facet/sites as the dominant active sites for the reaction. However, the commonly used method, plotting the TOF_{app} (based on all the exposed surface atoms) with the metal particle size, is effective to evaluate whether this reaction is structure sensitive or not, but it is difficult to reveal the origin of the structure sensitivity as well as the type, number and quality of the catalyst active sites. This is mainly because not all the exposed metal atoms are active for most catalytic reactions, and different crystal facets/sites usually have different catalytic activities. Notably, using this method to discriminate the dominant active sites for other and more complex cases, including Pt-catalyzed selective oxidation of glycerol and Pd-catalyzed selective hydrogenation of acetylene, is still

ongoing in our group.

4 Conclusions

In summary, we have successfully achieved the kinetics-assisted discrimination of dominant Ru active sites for the hydrolytic dehydrogenation of ammonia borane on hcp Ru/CNTs catalysts by combining multi-faceted kinetics analysis with model calculations. The size-insensitive activation energies indicated one typed Ru active sites as the dominant one for the reaction. According to the almost size-insensitive $TOF_{active\ site}$, the Ru edge atoms were discriminated as the dominant active sites, and the origin of the structure sensitivity mainly arised from the difference in the Ru geometric properties rather than that in the Ru electronic properties. On such active sites, the favorable occurrence of the rate-determining step was demonstrated by combining kinetic isotopic analysis with DFT calculations. These results demonstrate that the multi-faceted kinetics analysis followed by the model calculations are effective to discriminate the dominant active sites for the reaction, which could be applicable for other more complex structure-sensitive reactions.

Acknowledgements

This work was supported by the Natural Science Foundation of China (21776077), the Shanghai Natural Science Foundation (17ZR1407300 and 17ZR1407500), the Program for Professor of Special Appointment (Eastern Scholar) at Shanghai Institutions of Higher Learning, the Shanghai Rising-Star Program (17QA1401200), the Open Project of SKLOCE (SKL-Che-15C03), the State Key Laboratory of Organic-Inorganic

Composites (oic-201801007) and the 111 Project of the Ministry of Education of China (B08021).

References

1 M. Boudart, Catal. Lett., 2000, 65(1-3), 1-3.

2 W. Y. Chen, J. Ji, X. Feng, X. Z. Duan, G. Qian, P. Li, X. G. Zhou, D. Chen and W. K. Yuan, J. Am. Chem. Soc., 2014, 136(48), 16736-16739.

3 D. W. Blaylock, Y. A. Zhu and W. H. Green, Top. Catal., 2011, 54(13-15), 828.

4 C. Fan, Y. A. Zhu, M. L. Yang, Z. J. Sui, X. G. Zhou and D. Chen, Ind. Eng. Chem. Res., 2015, 54(22), 5901-5913.

5 Y. H. Chin, C. Buda, M. Neurock and E. Iglesia, J. Am. Chem. Soc., 2011, 133(40), 15958-15978.

6 J. X. Xie, J. Yang, A. I. Dugulan, A. Holmen, D. Chen, K. P. de Jong and M. J. Louwerse, ACS Catal., 2016, 6(5), 3147-3157.

7 X. Feng, X. Z. Duan, G. Qian, X. G. Zhou, D. Chen and W. K. Yuan, J. Catal., 2014, 317, 99-104.

8 L. Zhang, L. T. Roling, X. Wang, M. Vara, M. F. Chi, J. Y. Liu, S. Choi, J. Park, J. A. Herron, Z. X. Xie, M. Mavrikakis and Y. N. Xia, Science, 2015, 349(6246), 412-416.

9 B. Eren, D. Zherebetskyy, L. L. Patera, C. H. Wu, H. Bluhm, C. Africh, L. W. Wang, G. A. Somorjai and M. Salmeron, Science, 2016, 351(6272), 475-478.

10 F. Studt, I. Sharafutdinov, F. Abild-Pedersen, C. F. Elkjær, J. S. Hummelshoj, S. Dahl, I. Chorkendorff and J. K. Norskov, Nat. Chem., 2014, 6(4), 320.

11 H. Y. Ma and C. Z. Na, ACS Catal., 2015, 5(3), 1726-1735.

12 A. Staubitz, A. P. M. Robertson and I. Manners, Chem. Rev., 2010, 110(7), 4079-4124.

13 U. B. Demirci and P. Miele, Energ. Environ. Sci., 2009, 2(6), 627-637.

14 W. Y. Chen, D. L. Li, C. Peng, G. Qian, X. Z. Duan, D. Chen and X. G. Zhou, J. Catal., 2017, 356, 186-196.

15 W. Y. Chen, D. L. Li, Z. J. Wang, G. Qian, Z. J. Sui, X. Z. Duan, X. G. Zhou, I. Yeboah and D. Chen, AIChE J., 2017, 63(1), 60-65.

16 W. W. Zhan, Q. L. Zhu and Q. Xu, ACS Catal., 2016, 6(10), 6892-6905.

17 S. Akbayrak, Y. Tonbul and S. Özkar, Appl. Catal. B-Environ., 2016, 198, 162-170.

18 H. Yan, Y. Lin, H. Wu, W. H. Zhang, Z. H. Sun, H. Cheng, W. Liu, C. L. Wang, J. J. Li, X. H. Huang, T. Yao, J. L. Yang, S. Q. Wei and J. L. Lu, Nat. Commun., 2017, 8(1), 1070.

19 T. Karaca, M. Sevim and Ö. Metin, ChemCatChem, 2017, 9(22), 4185-4190.

20 W. Y. Chen, J. Ji, X. Z. Duan, G. Qian, P. Li, X. G. Zhou, D. Chen and W. K. Yuan,. Chem. Commun., 2014, 50(17), 2142-2144.

21 Z. Li, T. He, D. Matsumura, S. Miao, A. A. Wu, L. Liu, G. T. Wu and P. Chen, ACS Catal., 2017, 7(10), 6762-6769.

22 Z. Li, T. He, L. Liu, W. D. Chen, M. Zhang, G. T. Wu and P. Chen, Chem. Sci., 2017, 8(1), 781-788.

23 J. K. Zhang, W. Y. Chen, H. B. Ge, C. Q. Chen, W. J. Yan, Z. Gao, J. Gan, B. Y. Zhang, X. Z. Duan and Y. Qin, Appl. Catal. B-Environ., 2018, 235, 256-263.

24 W. Y. Chen, Z. J. Wang, X. Z. Duan, G. Qian, D. Chen and X. G. Zhou, Chem. Eng. Sci., 2018, 192, 1242-1251.

25 C. C. Hou, L. Li, C. J. Wang, C. Y. Peng, Q. Q. Chen, H. F. Ye, W. F. Fu, C. M. Che, N. López and Y. Chen, Energy Environ. Sci., 2017, 10(8), 1770-1776.

26 G. Z. Chen, R. Y. Wang, W. Zhao, B. T. Kang, D. W. Gao, C. C. Li and J. Y. Lee, J. Power Sources, 2018, 396, 148-154.

27 B. S. Zhang, W. Zhang and D. S. Su, ChemCatChem, 2011, 3(6), 965-968.

28 J. Wang, Z. Z. Wei, S. J. Mao, H. R. Li and Y. Wang, Energy Environ. Sci., 2018, 11(4), 800-806.

29 J. Mahmood, F. Li, S. M. Jung, M. S. Okyay, I. Ahmad, S. J. Kim, N. Park, H. Y. Jeong and J. B. Baek, Nature Nanotechnol., 2017, 12(5), 441.

30 Q. Zhang, K. Kusada, D. S. Wu, T. Yamamoto, T. Toriyama, S. Matsumura, S. Kawaguchi, Y. Kubota and H. Kitagawa, Nat. Commun., 2018, 9(1), 510.

31 V. Ragaini, R. Carli, C. L. Bianchi, D. Lorenzetti, G. Predieri and P. Moggi, Appl, Catal. A-Gen., 1996, 139(1-2), 31-42.

32 E. M. Simmons and J. F. Hartwig, Angew. Chem. Int. Ed.., 2012, 51(13), 3066-3072.